Spin dynamics in the quasi-one-dimensional $S=\frac{1}{2}$ antiferromagnet $BaCu_2Si_2O_7$

A. Zheludev*
Physics Department, Brookhaven National Laboratory, Upton, New York 11973-5000

M. Kenzelmann
Oxford Physics, Clarendon Laboratory, Oxford OX1 3PU, United Kingdom

S. Raymond
DRFMC/SPSMS/MDN, CENG, 17 rue des Martyrs, 38054 Grenoble Cedex, France

T. Masuda and K. Uchinokura
Department of Advanced Material Science, The University of Tokyo, 7-3-1 Bunkyo-ku, Tokyo 113-8656, Japan

S.-H. Lee
NIST Center for Neutron Research, National Institute of Standards and Technology, Maryland 20899
(Received 10 May 2001; published 29 November 2001)

Inelastic neutron scattering is used to identify single-particle and continuum spin excitations in the quasi-one-dimensional $S=1/2$ antiferromagnet $BaCu_2Si_2O_7$. In the data analysis, close attention is given to resolution effects. A gap in the continuum spectrum at $\Delta_c=4.8(2)$ meV is directly observed. The gap energy is in excellent agreement with existing theoretical predictions. Below the gap, the spectrum is dominated by sharp acoustic spin-wave excitations.

DOI: 10.1103/PhysRevB.65.014402 PACS number(s): 75.40.Gb, 75.10.Jm, 75.50.Ee

I. INTRODUCTION

Despite the apparent simplicity of the quantum $S=1/2$ antiferromagnetic (AF) Heisenberg model, the quest for a complete understanding of this system remains one of central problems in magnetism. Semiclassical spin-wave theory (SWT) is known to provide an adequate description of the three-dimensional (3D) version of the model. After extensive theoretical and experimental studies it is fair to say that the purely 1D case is rather well understood as well. Its static and dynamic properties totally defy the conventional spin-wave picture. In 1D the ground state looks nothing like the classical two-sublattice Néel state and is described as a ''marginal spin liquid,'' with power-law spatial spin correlations and no long-range order.[1] The spectrum contains no single-particle magnon excitation, but is instead a diffuse continuum described in terms of two-particle ''spinon'' states.[2–5] Of great current interest is the *quasi*-one-dimensional case of weakly interacting quantum spin chains. Studies of such systems provide the missing link between the exotic quantum-mechanical behavior of the 1D model and the more familiar semiclassical spin-wave dynamics realized in three dimensions.

A great deal of experimental information on the quasi-1D Heisenberg model was gained in studies of $KCuF_3$.[6–9] Particularly exciting was the recent observation of a novel longitudinal excitation, polarized along the direction of ordered moment and thus totally absent in SWT.[9] The recently characterized $BaCu_2Si_2O_7$ (Refs. 10–12) is another model weakly coupled chain compound, shown to be particularly useful for studying transverse spin fluctuations, i.e., those polarized perpendicular to the ordered moment. In a recent short paper[11] we have demonstrated that the transverse excitation spectrum in $BaCu_2Si_2O_7$ has a unique *dual* nature. At high energies the imaginary part of dynamic susceptibility is dominated by continuum excitations, characteristic of the quantum 1D model. However, at energies below the characteristic strength of interchain interactions, the continuum is ''cleaned up'' and replaced by sharp single-particle states, similar to conventional spin waves. A further analysis suggested that continuum excitations appear only above a well-defined threshold energy. Unfortunately, for purely technical reasons, this gap in the continuum could not be observed directly. In the present paper we report a detailed study of continuum excitations in the vicinity of the energy gap.

II. EFFECTIVE SPIN HAMILTONIAN FOR $BaCu_2Si_2O_7$

Before we proceed to describe the experimental procedures and results we shall briefly review the structure and relevant magnetic interactions in $BaCu_2Si_2O_7$, which are, by now, rather well documented. The silicate crystallizes in an orthorhombic structure, space group $Pnma$, with lattice constants are $a=8.862(2)$ Å, $b=13.178(1)$ Å, and $c=6.897(1)$ Å.[13] Magnetic properties are due to Cu^{2+} ions that form weakly coupled antiferromagnetic chains running along the crystallographic c axis. Correspondingly, the temperature dependence of bulk magnetic susceptibility follows the theoretical Bonner-Fisher curve[14] with an in-chain coupling $J=24$ meV.[10] A similar estimate was obtained in direct inelastic neutron scattering measurements of the 1D zone-boundary energy $\hbar\omega_{ZB}$ of magnetic excitations, related to J through $J=2\hbar\omega_{ZB}/\pi$.[15] This measurement gives $J=24.1$ meV.[12] Nearest-neighbor spin-spin separation within the chains is equal to $c/2$, so the 1D AF zone center $q_\parallel=\pi$

corresponds to $l=1$, where $\boldsymbol{Q}=(h,k,l)$ denotes a wave vector in reciprocal space.

Weak interactions between the chains result in long-range antiferromagnetic ordering at $T_N=9.2$ K.[10] The ordered moment is parallel to the chain axis and extrapolates to a saturation value of 0.15 μ_B at $T\rightarrow 0$.[10–12] In the ordered state the alignment of nearest-neighbor spins is parallel along the *a* and antiparallel along the *b* and *c* directions, respectively. The 3D AF zone center is located at $\boldsymbol{Q}=(0,1,1)$. The relevant interchain exchange constants were determined from measurements of spin-wave dispersion along several directions in reciprocal space.[12] The effective spin Hamiltonian was established:

$$H=\sum_{i,j,n} J\boldsymbol{S}_{i,j,n}\boldsymbol{S}_{i,j,n+1}+J_x\boldsymbol{S}_{i,j,n}\boldsymbol{S}_{i+1,j,n}+J_y\boldsymbol{S}_{i,j,n}\boldsymbol{S}_{i,j+1,n}+J_3\boldsymbol{S}_{i,j,n}\boldsymbol{S}_{i+1,j+1,n}+J_3\boldsymbol{S}_{i,j,n}\boldsymbol{S}_{i+1,j-1,n}. \quad (1)$$

Here the sum is taken over all spins in the system. The indexes *i* and *j* enumerate the spin chains along the *a* and *b* axes, respectively, and *n* labels the spins within each chain. The experimental values of the interchain exchange parameter are[12]

$$J_x=-0.460(7)\ \text{meV},$$

$$J_y=0.200(6)\ \text{meV},$$

$$2J_3=0.152(7)\ \text{meV}. \quad (2)$$

The spin chains in $BaCu_2Si_2O_7$ are not straight, but slightly zigzag. The magnetic sites are displaced from high-symmetry $(\frac{1}{4},0,\frac{1}{4})$ positions as described in Ref. 10. For the neutron scattering measurements described below, this fact has one unfortunate consequence. The 3D magnetic dynamic structure factor $S(\boldsymbol{Q},\omega)$ probed experimentally is not that of an ideal straight chain, $S_0(\boldsymbol{Q},\omega)$, but related to it through the following rather complicated relation:

$$\begin{aligned}S(\boldsymbol{Q},\omega)=&\cos^2(2\pi h\delta_x)\cos^2(2\pi k\delta_y)\cos^2(2\pi l\delta_z)S_0(\boldsymbol{Q},\omega)+\cos^2(2\pi h\delta_x)\cos^2(2\pi k\delta_y)\sin^2(2\pi l\delta_z)S_0(\boldsymbol{Q}+(100),\omega)\\&+\cos^2(2\pi h\delta_x)\sin^2(2\pi k\delta_y)\cos^2(2\pi l\delta_z)S_0(\boldsymbol{Q}+(011),\omega)+\cos^2(2\pi h\delta_x)\sin^2(2\pi k\delta_y)\sin^2(2\pi l\delta_z)\\&\times S_0(\boldsymbol{Q}+(111),\omega)+\sin^2(2\pi h\delta_x)\cos^2(2\pi k\delta_y)\cos^2(2\pi l\delta_z)S_0(\boldsymbol{Q}+(001),\omega)\\&+\sin^2(2\pi h\delta_x)\cos^2(2\pi k\delta_y)\sin^2(2\pi l\delta_z)S_0(\boldsymbol{Q}+(101),\omega)+\sin^2(2\pi h\delta_x)\sin^2(2\pi k\delta_y)\cos^2(2\pi l\delta_z)\\&\times S_0(\boldsymbol{Q}+(010),\omega)+\sin^2(2\pi h\delta_x)\sin^2(2\pi k\delta_y)\sin^2(2\pi l\delta_z)S_0(\boldsymbol{Q}+(110),\omega). \quad (3)\end{aligned}$$

In this equation $\delta_x\approx 0.028$, $\delta_y\approx 0.004$, and $\delta_z\approx 0.044$ are Cu^{2+} displacements from high-symmetry positions as described in Ref. 10 and 18. It is important to emphasize that Eq. (3) is an exact result. At small wave vectors only the first term is relevant and the dynamic structure factor is that of a straight chain. Indeed, the straight-chain model could be successfully used to analyze the data in previous studies.[11,12] Below we shall demonstrate that at higher wave vector transfers the contributions of other terms become significant and should be taken into account explicitly.

III. EXPERIMENTAL PROCEDURES

The main goal of the present work was to reliably resolve low-energy spin wave and continuum excitations near the 1D AF zone center in $BaCu_2Si_2O_7$. Previous studies indicated that in $BaCu_2Si_2O_7$ the continuum sets in between 3.5 meV and 5.5 meV energy transfer.[11] The most interesting dynamic range is therefore between zero and 10 meV. The choice of spectrometer configurations in inelastic neutron scattering experiments was therefore governed by the conflicting needs of intensity, high wave vector resolution along the chain axis (required to overcome the steep dispersion along the chains), energy resolution, and the need to cover a wide range of energy transfers. Since it appears impossible to simultaneously satisfy all these conditions, several different experimental setups with complementary characteristics were utilized. Quantitative comparisons between data sets collected in different configurations were essential to verifying the validity of the results. In all cases we used the same $BaCu_2Si_2O_7$ single-crystal sample as in previous studies.[11,12] In all configurations the crystal was mounted with the $(0,k,l)$ reciprocal-space plane in the scattering plane of the spectrometer.

Ideally, the measurements are done around $\boldsymbol{Q}=(0,0,1)$ $(q_\parallel=\pi)$, where the extra terms in Eq. (3) are negligible and all magnetic scattering is due to spin fluctuations transverse to the direction of the ordered moment (*c* axis). Unfortunately, at this wave vector, certain geometric constraints restrict the accessible range of energy transfers to just over 4 meV. Measurements in this range were performed on the IN14 cold-neutron spectrometer installed at Institute Laue-Langevin (ILL), using a very high energy and wave vector resolution configuration (setup I): guide-40′-40′-open collimations, $E_f=3$ meV fixed final-energy neutrons, and a Be filter after the sample. To cover a wider energy range and still have reasonable wave vector and energy resolutions we employed IN14 in ''anti-W'' geometry with guide-

40′-60′-open collimations and final neutron energy fixed at $E_f = 5$ meV (setup II). The data were collected around $\boldsymbol{Q} = (0,0,3)$ ($q_\parallel = 3\pi$), where the contributions of both the first and second terms in Eq. (3) are significant. In this geometry measurements could be extended up to 8 meV energy transfer. A similar configuration was used in combination with a horizontally focusing analyzer (setup III). While in this latter mode the wave vector resolution is considerably worse than with a flat analyzer, the intensity gain is quite substantial. Energy transfers of up to 17 meV were achieved using the IN22 spectrometer at ILL, with guide-60′-60′-open collimations and final neutron energy fixed at $E_f = 14.7$ meV (setup IV). In this case a pyrolitic graphite (PG) filter was used after the sample.

In all experiments sample environment was a standard ''ILL Orange'' He-4 cryostat and all data were collected at either $T = 1.5$ K or $T = 2$ K. For the cold-neutron experiments the background was measured in constant-Q scans, away from the 1D AF zone center, where no magnetic scattering is expected to occur, due to a step dispersion along the chain axis. In all cases the background was found to be completely flat and featureless, typically 2.5, 4, and 5 counts per minute for setups I, II, and III, respectively. The measured background was fit to a straight line and is subtracted from all the data sets shown below. For the thermal-neutron experiment (setup IV) the background was measured on an empty sample can and subtracted from the experimental data in a similar fashion.

IV. RESULTS

A. Transverse spin excitations

Representative constant-Q scans measured at the 1D AF zone center $q_\parallel = \pi$, 3π using Setups I, II, and III are shown in Fig. 1. To the right of each scan we plot the calculated full width at half maximum (FWHM) resolution ellipsoids in projection on the $(l,\hbar\omega)$ plane to show their size and orientation relative to the spin-wave dispersion branches originating from the first and second terms in Eq. (3) (solid lines). Three distinct components of the excitation spectrum are apparent. The sharp peak at $\hbar\omega \approx 2$ meV is the single-particle spin-wave mode given by the first term in Eq. (3). This feature dominates the low-energy spectrum around $\boldsymbol{Q} = (0,0,1)$, where the other terms in Eq. (3) are negligible thanks to the small value of corresponding trigonometric prefactors [Fig. 1(a) and Figs. 1 and 2 in Ref. 11]. At $q_\parallel = 3\pi$, however, the second term in Eq. (3) becomes significant and gives rise to the 3 meV peak in Figs. 1(b) and 1(c), which was not observed in previous studies. In essence, this second peak is an ''echo'' of the same spin-wave excitation visible by virtue of a nontrivial 3D arrangement of magnetic sites. The third feature in Fig. 1 is the diffuse scattering above the spin-wave peaks that, as will be discussed in detail below, is not a resolution-enhanced ''tail'' of the spin-wave peaks, but a separate entity. This scattering is attributed to continuum excitations in the system. In Figs. 1(b) and 1(c) one can see a weak yet reproducible intensity dip that separates this continuum scattering from the underlying spin waves (arrows).

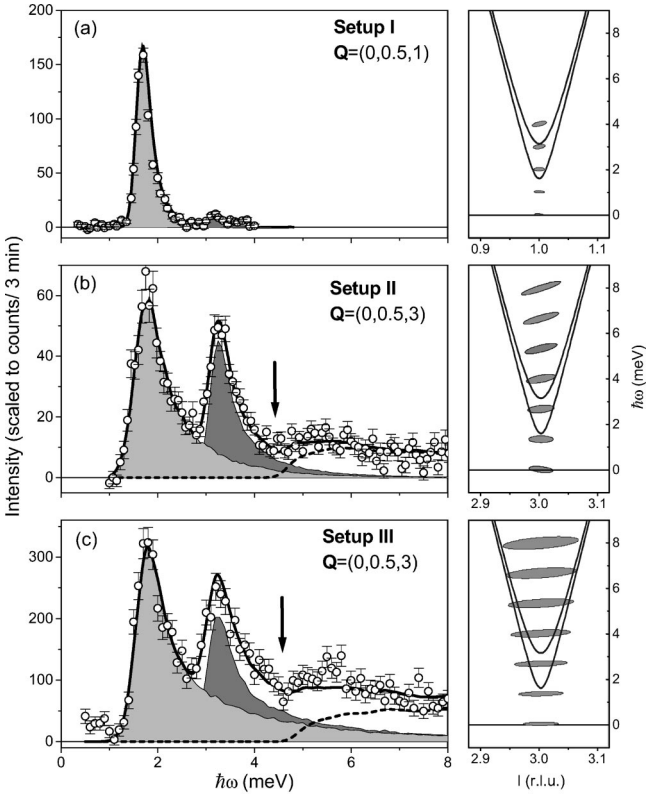

FIG. 1. Left: typical constant-Q scans collected in $BaCu_2Si_2O_7$ at the 1D AF zone center using different spectrometer configurations. Heavy solid lines represent a semiglobal fit to the data as described in the text. Shaded areas are contributions of single-particle excitations given by Eqs. (4) and (5). Dashed lines show the continuum contribution, as expressed by Eq. (10). Arrows indicate the slight dip in the observed intensity that corresponds to the continuum energy gap Δ_c. Right: evolution of the calculated FWHM resolution ellipsoids in the course of the corresponding scans, plotted in projection onto the $(l,\hbar\omega)$ plane. Solid lines represent the spin-wave dispersion relation.

Figure 2 shows constant-Q scans collected with setup III at different wave vector transfers perpendicular to the chains. The dispersion of the lower-energy spin wave is quite apparent. An almost total absence of dispersion in the 3 meV peak is consistent with that it originates from $\boldsymbol{Q} + (100)$ scattering [Eq. (3)] and the known spin-wave dispersion along the $(1,k,1)$ reciprocal-space rod (Ref. 12, Fig. 6). In all cases the continuum is observed, and the intensity dip occurs at roughly the same energy (arrows). There seems to be no obvious wave vector dependence of the continuum intensity along the b^* direction. The energy resolution of the thermal-neutron experiment (setup IV) is too coarse to resolve the two spin-wave branches and the continuum. Figure 3 shows an energy scans collected in this configuration at $\boldsymbol{Q} = (0,0,3)$.

Several constant-E scans measured with different configurations are shown in Fig. 4. At 3 meV energy transfer [Fig. 4(a)] two spin-wave peaks are perfectly resolved using the highest-resolution configuration (setup I). This proves that at these energies the excitation spectrum is entirely due to single-particle excitations. At the same energy transfer

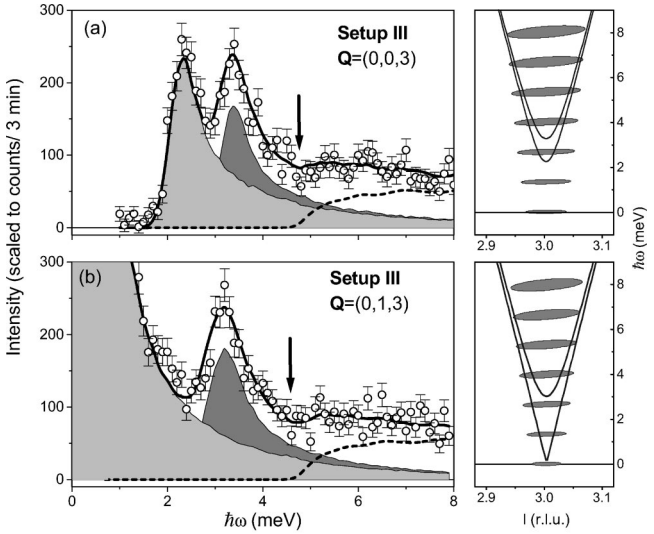

FIG. 2. Constant-Q scans collected in $BaCu_2Si_2O_7$ at the 1D AF zone center at different momentum transfers perpendicular to the chains using setup III. Lines, shaded areas, and graphical representations of the resolution functions on the left are as in Fig. 1.

setup II lacks the wave vector resolution to resolve the spin-wave peaks, as can be seen from Fig. 4(b). However, as will be discussed in detail in the next section, at higher energies [Figs. 4(c) and 4(d)], while the resolution is sufficient to resolve individual spin-wave peaks, only a single broad feature is observed. As explained in Ref. 11, this behavior is a result of the excitation continuum ''filling in'' the space between the spin-wave branches. The trend continues at even higher energies, as can be seen from Figs. 4(e) and 4(f), which show scans collected using setup IV.

B. Data analysis

Resolution effects, particularly wave vector resolution along the chain axis, are clearly a major factor in the experiments discussed here. In order to reliably distinguish between continuum scattering and the high-energy resolution ''tails'' of the single-particle peaks, one has to deconvolute the signal and the resolution function of the spectrometer. In practice this is done by constructing a parametrized model cross section, numerically convoluting it with the calculated

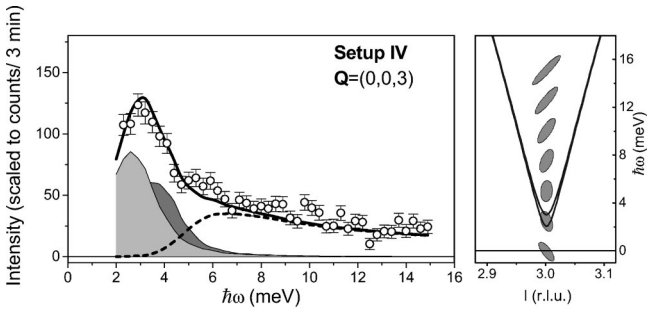

FIG. 3. Constant-Q scan collected in $BaCu_2Si_2O_7$ at the 1D AF zone center using the thermal-neutron setup IV. Lines, shaded areas, and graphical representation of the resolution function on the left are as in Fig. 1.

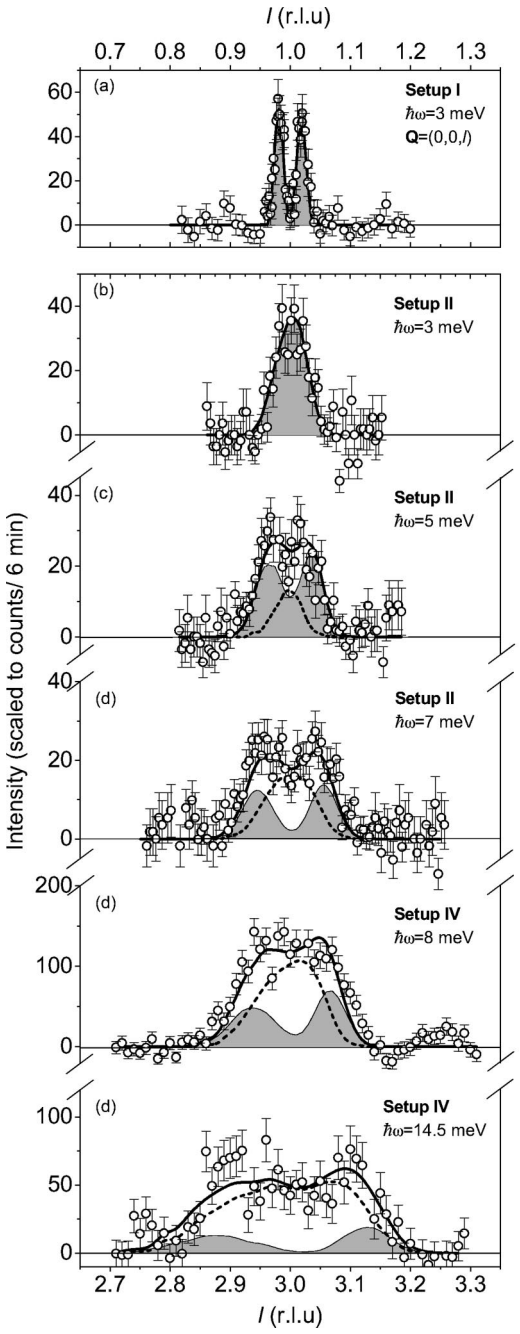

FIG. 4. A series of constant-E scans along the spin chains in $BaCu_2Si_2O_7$. Lines and shaded areas are as in Fig. 1.

resolution and adjusting the parameters to best fit the data. Confidence in this procedure can be gained by *simultaneously* fitting data sets collected in spectrometer configurations with different resolution characteristics, while using the *same* model cross section function and parameters.

1. Model cross section function

A simple yet accurate description of the spin dynamics in weakly interacting Heisenberg chains is provided by the mean-field and random phase approximation (MF-RPA) treatment of interchain interactions.[16,17] Within this frame-

work, the $T=0$ transverse-polarized spectrum of a weakly ordered quasi-1D $S=1/2$ system has two distinct contributions.

The first contribution is from transverse-polarized single-particle excitations (spin waves), associated with the presence of long-range antiferromagnetic order. For $BaCu_2Si_2O_7$ the spin-wave dispersion has been investigated in some detail[12] and found to be in excellent agreement with MF-RPA theoretical predictions. In the present work we shall employ the same expression for the spin-wave structure factor, as in Ref. 12:

$$S^{xx}_{\mathrm{SM},0}(\boldsymbol{Q},\omega)=A\frac{[1-\cos(\pi l)]}{2}\delta[\omega^2-\omega_x^2(\boldsymbol{Q})], \tag{4}$$

$$S^{yy}_{\mathrm{SM},0}(\boldsymbol{Q},\omega)=A\frac{[1-\cos(\pi l)]}{2}\delta[\omega^2-\omega_y^2(\boldsymbol{Q})], \tag{5}$$

$$[\omega_{x,y}(\boldsymbol{Q})]^2=\frac{\pi^2}{4}J^2\ \sin^2(\pi l)+\frac{\Delta^2}{|J'|}[|J'|+J(\boldsymbol{Q})]+D_{x,y}^2, \tag{6}$$

$$|J'|\equiv\frac{1}{2}(|J_x|+|J_y|+2|J_3|). \tag{7}$$

In this formula $S^{xx}_{\mathrm{SM},0}(\boldsymbol{Q},\omega)$ and $S^{xx}_{\mathrm{SM},0}(\boldsymbol{Q},\omega)$ are single-mode (SM) dynamic structure factors for excitations polarized along the *a* and *b* axes, respectively, assuming *straight* spin chains in the system. The actual SM structure factors $S^{xx}_{\mathrm{SM}}(\boldsymbol{Q},\omega)$ and $S^{yy}_{\mathrm{SM}}(\boldsymbol{Q},\omega)$ for the zigzag chain in $BaCu_2Si_2O_7$ are related to $S^{xx}_{\mathrm{SM},0}(\boldsymbol{Q},\omega)$ and $S^{yy}_{\mathrm{SM},0}(\boldsymbol{Q},\omega)$ through Eq. (3). The parameter A in Eq. (7) represents an overall intensity prefactor, while $D_x=0.36$ meV and $D_y=0.21$ meV (Ref. 12) are anisotropy gaps for the two spin-wave branches. In Eq. (7), $J(\boldsymbol{Q})$ is the Fourier transform of interchain coupling and is given by

$$J(\boldsymbol{Q})=2J_x\ \cos(\pi h)+2J_y\ \cos(\pi k)+2J_3\ \cos[\pi(h+k)]+2J_3\ \cos[\pi(h-k)]. \tag{8}$$

The ''mass gap'' Δ in Eq. (7) defines the bandwidth of spin-wave dispersion perpendicular to the chains. Its physical meaning deserves some comment. In the chain-MF model, in the magnetically ordered state, each spin chain experiences an effective staggered field H_π generated by the static staggered magnetization in adjacent chains. The staggered field produces a confining potential between spinons in an $S=1/2$ chain, yielding a two-spinon bound state.[16] This new single-particle excitation has a gap Δ that scales as $\Delta\propto H_\pi^{2/3}$.[19] When interchain interactions are switched on at the RPA level, the bound state acquires a dispersion perpendicular to the chain axis and takes the role of a conventional spin wave. At the 3D AF zone center (the location of magnetic Bragg reflections) its energy goes to zero, as appropriate for a Goldstone mode. The mass gap Δ still enters the dispersion relation, as in Eq. (7). It is directly related to the strength of interchain interactions through[16]

$$\Delta\approx 6.175|J'|. \tag{9}$$

From the known values of interchain coupling constants for $BaCu_2Si_2O_7$ one gets[12] $\Delta=2.51$ meV.[20]

The second contribution to the transverse dynamic structure factor in the MF-RPA model is what remains of the two-spinon continuum in isolated chains.[16,17] Unfortunately, a convenient analytical expression for this diffuse part of cross section, one that could be used to analyze the data, is not currently available. In our analysis we instead employed a simple ansatz that has the same main characteristics as the MF-RPA result: (i) At high energies the Muller-ansatz form that describes two-spinon continuum scattering in isolated chains[22] is recovered. (ii) The continuum has a sharp step-function low-energy cutoff (gap) $\Delta_c=2\Delta$ at the 1D AF zone center $q_\parallel=\pi$. (iii) Unlike the spin waves, the lower continuum bound shows no dispersion perpendicular to the chain axis. (iv) The $q_\parallel$ dependence of the lower bound is given by $[\Delta_c(q_\parallel)]^2=\Delta_c^2+(\pi^2/4)J^2\ \sin^2(q_\parallel)$. And (v) except at the ''magic'' reciprocal-space point $(0.5,0.5,1)$, where interchain interactions cancel out at the RPA level, the continuum has no singularity at the lower bound. To analyze our data, where none of the measured scans were taken in the vicinity of the magic wave vector, we used the following empirical function to model the continuum part of the dynamic structure factor:

$$S^{xx,yy}_{\mathrm{c},0}(\boldsymbol{Q},\omega)=\alpha A\frac{[1-\cos(\pi l)]}{2}\times\frac{1}{\sqrt{\omega^2-\frac{\pi^2}{4}J^2\ \sin^2(q_\parallel)}}\theta[\omega-\omega_c(\boldsymbol{Q})], \tag{10}$$

$$[\omega_c(\boldsymbol{Q})]^2=\Delta_c^2+\frac{\pi^2}{4}J^2\ \sin^2(\pi l). \tag{11}$$

The parameter α is the intensity of continuum scattering relative to that of the spin waves, and $\theta(x)$ is the Heaviside step function. In essence, Eq. (10) is simply the Müller ansatz truncated at the expected lower continuum bound. For the 3D spin arrangement in $BaCu_2Si_2O_7$ the actual continuum cross sections $S_{\mathrm{c}}^{xx,yy}$ are related to $S_{\mathrm{c},0}^{xx,yy}$ through Eq. (3).

2. Choice of adjustable parameters

The goal was to perform a global analysis of all data sets collected in different configurations using as few adjustable parameters as possible. All relevant exchange constants and anisotropy parameters have been measured previously.[12] These constants were fixed to the values quoted in Sec. II. Since we have not performed absolute calibration of intensities measured in various setups, a separate value of the intensity prefactor A was used for each configuration. However, the same values of A were used for different scans measured using the same setup. In our analysis the con-

tinuum gap Δ_c was used as a separate variable, independent of Δ. As with the continuum intensity prefactor α, the same value of Δ_c was used for all data sets measured in all configurations.

In Eq. (3) only the first two terms were found to be of any significance for the particular experiment, where the data were collected at small momentum transfers along the *a* and *b* axes. Equation (3) could thus be greatly simplified by setting the transverse zigzag displacements δ_x and δ_y to zero. The relevant longitudinal displacement parameter δ_z can be expected to have a slight temperature dependence. Only the room-temperature value $\delta_z=0.044$ is known from structural data,[13] and in our analysis it had to be treated as an adjustable variable. The same value of δ_z was used for all data sets simultaneously.

3. Fits to experimental data

All together, nine constant-Q and eight constant-E scans were analyzed, including all those shown in Figs. 1–4. The model cross section, defined by Eqs. (7)–(11) and Eq. (3), was numerically folded with the calculated Cooper-Nathans resolution functions[23] for each setup. The calculation was based on the known geometry of the spectrometers and characteristics of the neutron guides, monochromator and analyzer crystals, and collimators used in the experiments. The reliability of the resolution calculation was checked against the measured energy widths of elastic incoherent scattering from the sample in each setup. The folded cross section was scaled by the square of the magnetic form factor of Cu^{2+} and fit to the data using a least-squares algorithm.

The result of the fit ($\chi^2=1.7$) is shown as solid lines in Figs. 1–4. The shaded areas are contributions of the single-mode part of the cross section. In the constant-energy scans the contributions of the spin-wave branches, originating from the first two terms in Eq. (3), are merged into a single profile. These two contributions are shown in shading of different intensity in the constant-Q data. The dashed lines represent the continuum part of the cross section. The following fit parameters were obtained: $\Delta_c=4.8(2)$ meV, $\alpha=0.41(3)$, and $\delta_z=0.041(1)$.

It is gratifying to see that the model fit function reproduces the available data extremely well with just a few parameters. The refined value for δ_z is very close to its room-temperature value. The fitted continuum gap Δ_c is within the error bar of the chain-RPA result: $\Delta_c=2\Delta=5.0$ meV.

To extract information on the excitation continuum without having to rely on a specific ansatz to describe its shape, we employed an alternative data analysis procedure. The data collected in constant-Q scans using setup III below 3.5 meV were fit using only the SM part of the model cross section function ($\chi^2=1.2$). The result was then used to simulate the SM contribution in the entire scan range and subtracted from the measured data. The remaining intensity is due to continuum scattering and is shown in Fig. 5, where the results obtained at $\boldsymbol{Q}=(0,0,3)$, $(0,0.5,3)$, and $(0,1,3)$ have been averaged. In this plot the threshold at around $2\Delta=5$ meV becomes clearly apparent. It is important to stress the difference between Fig. 5 and Fig. 4 of Ref. 11: the latter

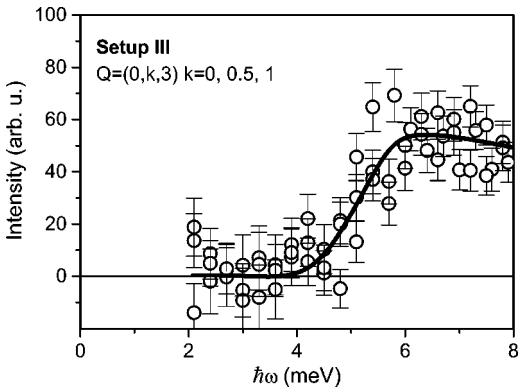

FIG. 5. Measured intensity of transverse-polarized continuum scattering in $BaCu_2Si_2O_7$, obtained by subtracting the simulated single-mode contribution from constant-Q scans as explained in the text. The solid line is a guide for the eye.

is a plot of the $q_\parallel$-*integrated* intensity, while the former is obtained from constant-Q scans at the 1D AF zone center. In a constant-Q scan the influence of the single-particle part is less significant at higher energies than in a q_z-integrated measurement, and the continuum is more easily observed.

C. Attempt to observe the longitudinal mode

One of the most interesting predictions of the MF-RPA model for weakly coupled $S=1/2$ Heisenberg chains is the so-called longitudinal mode: a single-particle excitation polarized along the direction of ordered moment. This unique feature is totally absent in conventional spin-wave theory, where the excitations represent the *precession* of the order parameter around its equilibrium direction and are thus transverse polarized. The longitudinal mode has been recently observed in the quasi-1D $S=1/2$ system $KCuF_3$ by means of unpolarized[9] and polarized[24] inelastic neutron scattering. In addition to the study of transverse-polarized excitations in $BaCu_2Si_2O_7$, we performed a dedicated experiment to search for the longitudinal mode in this system.

MF-RPA theory makes specific predictions for the energy and intensity of the longitudinal mode. Unlike the transverse spin waves that have a substantial dispersion perpendicular to the chains and reach zero energy at the 3D AF zone center, the longitudinal mode is gapped and has very little dispersion in this direction. Its RPA dynamic structure factor can be written as[17]

$$S^{zz}_{\mathrm{SM},0}(\boldsymbol{Q},\omega)=A\frac{\gamma}{2}\frac{[1-\cos(\pi l)]}{2}\delta[\omega^2-\omega_z^2(\boldsymbol{Q})], \quad (12)$$

$$[\omega_z(\boldsymbol{Q})]^2=\frac{\pi^2}{4}J^2\sin^2(\pi l)+\frac{\Delta^2}{|J'|}[3|J'|+J(\boldsymbol{Q})], \quad (13)$$

$$\gamma\approx 0.49. \quad (14)$$

From these equations we see that the longitudinal mode is expected to have a gap of $\sqrt{3}\Delta$ and be approximately 4 times weaker in intensity than the transverse-polarized spin waves.

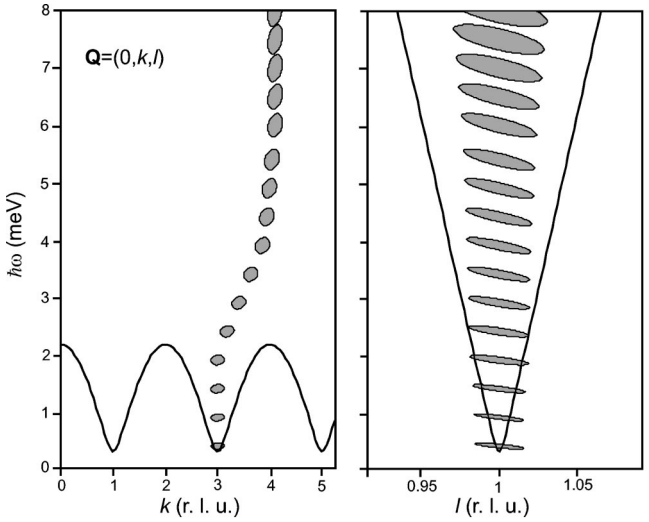

FIG. 6. Reciprocal space and energy trajectory of the inelastic scan measured in $BaCu_2Si_2O_7$ using setup V, showing the orientation of FWHM resolution ellipsoids relative to the spin-wave dispersion.

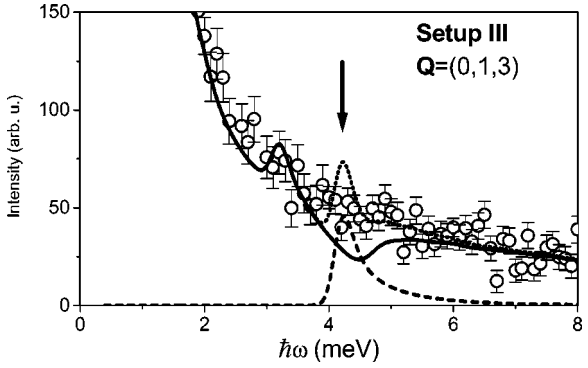

FIG. 7. Constant-$q_\parallel$ scan collected in $BaCu_2Si_2O_7$ at the 1D AF zone center and large momentum transfer perpendicular to the chains, using setup V. The trajectory of the scan is as shown in Fig. 6. The solid line is an estimate of the contribution of spin fluctuation perpendicular to the direction of ordered moment. The dashed line shows the expected contribution of the longitudinal mode, as predicted by the MF-RPA model (Ref. 17). The dotted line is the MF-RPA prediction for the total scattering intensity.

To look for the longitudinal mode in $BaCu_2Si_2O_7$, measurements were performed at large momentum transfers perpendicular to the chain axis. In this geometry the angle between the ordered moment (c axis) and the scattering vector is large, and both longitudinal and transverse excitations contribute to scattering. The data were collected at the NG5 cold three-axis spectrometer at the National Institute of Standards and Technology Center for Neutron Research. The large momentum transfers perpendicular to the chains enabled us to take full advantage of a horizontally focusing PG analyzer. The chain axis was at all times aligned as closely parallel to the scattered beam as possible, ensuring that energy and c-axis wave-vector resolution widths remained at least as narrow as in the standard flat-analyzer mode. The data were thus collected along a rather nontrivial trajectory in E-Q space, as illustrated in Fig. 6. At all times the momentum transfer along the chains was maintained at the 1D AF zone center $l=1$. Neutrons of $E_f=5$ meV were used with a Be filter positioned after the sample and guide-80′-80′ (radial)-open collimations (setup V). The background (flat, 3.4 counts/min) was measured by repeating the scan with the sample rotated by roughly 20° around the a axis.

The data are shown in Fig. 7. At low energies, below 3 meV energy transfer, we expect the main contribution to the scattering intensity to originate from the gapless transverse-polarized spin waves. After the inclusion of appropriate neutron polarization factors, the cross section for transverse excitations described above was fit to this low-energy portion of the scan (up to 3 meV transfer). All parameters, including Δ_c and α, were fixed at the values determined previously, and only the intensity prefactor was treated as an adjustable variable. The result of the fit is shown in a solid line in Fig. 7. We see that the transverse-polarized cross section alone reproduces the measured scan rather well. The only inconsistency is the lack of a dip or even inflection point in the measured intensity at Δ_c. However, the fit shows that experimental energy resolution should have been sufficient to resolve it.

In principle, one could subtract the fit from the experimental data and claim that the residual intensity is due to longitudinal spin fluctuation. Given the severity of resolution effects, we were reluctant to push the data analysis to this level. What we did instead was simulate the expected contribution from the longitudinal mode, as given by Eq. (14) and an appropriate neutron polarization factor, and shown in a dashed line in Fig. 7. Note that the ''extra'' intensity (arrow in Fig. 7), not accounted for by the transverse dynamic structure factor, is centered at roughly the same energy as the expected longitudinal excitation. Moreover, the intensity ''surplus,'' integrated in the range 3.5–5.5 meV [3.0(0.4) counts/(min meV)], is within the error bar of the expected intensity of the longitudinal mode integrated in this range [2.7 counts/(min meV)]. If the longitudinal mode was a sharp single-particle excitation, as predicted by the RPA, a well-defined peak centered at 4.2 meV should have been easily observed with our experimental statistics. This is illustrated by the dotted line, which is the calculated sum of the transverse contribution obtained in the fit and that given by Eq. (14) for the longitudinal mode. The result can be reconciled with the RPA model, if one assumes that the longitudinal mode has a finite lifetime, i.e., an intrinsic energy width of roughly 1 meV. This scenario would explain both the ''extra'' intensity and the absence of a sharp peak. It is also consistent with experimental studies of $KCuF_3$,[9] where the observed longitudinal mode *is* broadened and has an intrinsic width of roughly 1/4 of its central energy.

V. DISCUSSION AND CONCLUDING REMARKS

Despite the obvious difficulties associated with wave vector and energy resolution, the $BaCu_2Si_2O_7$ data presented above contain compelling evidence for a gap, or at least a *pseudogap*, in the transverse-polarized continuum. The gap

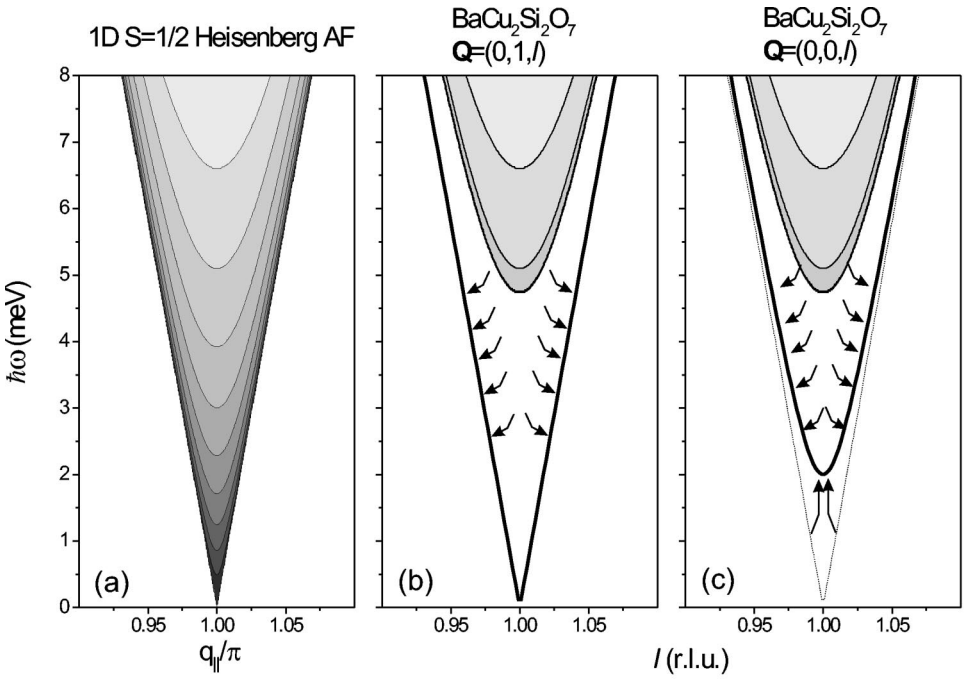

FIG. 8. Redistribution of spectral weight in a 1D $S=1/2$ Heisenberg AF (a) that occurs when interchain interactions are switched on, as in $BaCu_2Si_2O_7$ (b), (c).

value $\Delta_c = 4.8$ meV$\approx 2\Delta$ is in excellent agreement with predictions of the MF-RPA model. Interestingly, nonlinear spin-wave theory[25] (NSWT) predicts a much larger threshold energy. In this model the lowest-energy transverse-polarized continuum excitations are three-magnon states, and a pseudogap occurs at roughly 3Δ. An NSWT calculation for $BaCu_2Si_2O_7$ based on the known exchange parameters gives $\Delta_c \approx 7.5$ meV.[11]

Figure 8 is a cartoon illustration of how the spectral weight of transverse-polarized excitations gets redistributed in a 1D $S=1/2$ Heisenberg AF when interchain interactions are switched on. The singularity on the lower bound in the 1D system [Fig. 8(a)] becomes separated from the bulk of the two-spinon continuum [Fig. 8(b) and 8(c)]. The spectral weight in its vicinity is consolidated (arrows) to yield a sharp spin-wave excitation (solid lines).

Our results regarding longitudinal excitations are less conclusive. Clearly, additional measurements, possibly using polarized neutrons, will be required to fully resolve this problem for $BaCu_2Si_2O_7$. The available unpolarized data shown above are, in fact, consistent with the MF-RPA model, but suggest a finite lifetime for the longitudinal mode, as in $KCuF_3$.[9]

ACKNOWLEDGMENTS

We would like to thank I. Tsukada, Y. Sasago, and K. Kakurai for cooperation in earlier stages of this project, Dr. L. P. Regnault (CEA Grenoble) and Dr. A. Wildes for their assistance with experiments at ILL, and Professor F. H. L. Essler (University of Warwick), Professor R. A. Cowley (Oxford University), and Dr. I. Zaliznyak (BNL) for illuminating discussions. This work was supported in part by the U.S.-Japan Cooperative Program on Neutron Scattering, Grant-in-Aid for COE Research ''SCP coupled system'' of the Ministry of Education, Science, Sports, and Culture. Work at Brookhaven National Laboratory was carried out under Contract No. DE-AC02-98CH10886, Division of Material Science, U.S. Department of Energy. One of the authors (M.K.) was supported by the Swiss National Science Foundation under Contract No. 83EU-053223. Studies at NIST were partially supported by the NSF under Contract No. DMR-9413101.

*Present address: Solid State Division, Oak Ridge National Laboratory, Oak Ridge, TN 37831-6393.

[1] H.A. Bethe, Z. Phys. **71**, 256 (1931).

[2] L.D. Fadeev and L.A. Takhtajan, Phys. Lett. **85A**, 375 (1981).

[3] F.D.M. Haldane and M.R. Zirnbauer, Phys. Rev. Lett. **71**, 4055 (1993).

[4] G. Muller, H. Thomas, M.W. Puga, and H. Beck, J. Phys. C **14**, 3399 (1981).

[5] M. Karbach, G. Muller, A.H. Bougourzi, A. Fledderjohann, and K.-H. Mutter, Phys. Rev. B **55**, 12 510 (1997).

[6] S.K. Satija, J.D. Axe, G. Shirane, H. Yoshizawa, and K. Hirakawa, Phys. Rev. B **21**, 2001 (1980).

[7] S.E. Nagler, D.A. Tennant, R.A. Cowley, T.G. Perring, and S.K. Satija, Phys. Rev. B **44**, 12 361 (1991); D.A. Tennant, T.G. Perring, R.A. Cowley, and S.E. Nagler, Phys. Rev. Lett. **70**, 4003 (1993).

[8] D.A. Tennant, S.E. Nagler, D. Welz, G. Shirane, and K. Yamada, Phys. Rev. B **52**, 13 381 (1995).

[9] B. Lake, D.A. Tennant, and S.E. Nagler, Phys. Rev. Lett. **85**, 832 (2000).

[10] I. Tsukada, Y. Sasago, K. Uchinokura, A. Zheludev, S. Maslov, G. Shirane, K. Kakurai, and E. Ressouche, Phys. Rev. B **60**, 6601 (1999).

[11] A. Zheludev, M. Kenzelmann, S. Raymond, E. Ressouche, T. Ma-

suda, K. Kakurai, S. Maslov, I. Tsukada, K. Uchinokura, and A. Wildes, Phys. Rev. Lett. **85**, 4799 (2000).

[12] M. Kenzelmann, A. Zheludev, S. Raymond, E. Ressouche, T. Masuda, P. Bni, K. Kakurai, I. Tsukada, K. Uchinokura, and R. Coldea, Phys. Rev. B **64**, 054422 (2001).

[13] J.A.S. Oliveira, Ph.D. thesis, Ruprecht-Karls-Universitat, Heidelberg, 1993.

[14] J.C. Bonner and M.E. Fisher, Phys. Rev. **135**, A640 (1964).

[15] J. des Cloizeaux and J.J. Pearson, Phys. Rev. **128**, 2131 (1962).

[16] H.J. Schulz, Phys. Rev. Lett. **77**, 2790 (1996).

[17] F.H.L. Essler, A.M. Tsvelik, and G. Delfino, Phys. Rev. B **56**, 11 001 (1997).

[18] We found that Eq. (8) in Ref. 10 is incorrect. Equation (3) is the corrected version of this formula, rewritten to take δ_y into account.

[19] M. Oshikawa and I. Affleck, Phys. Rev. Lett. **79**, 2883 (1997).

[20] It has recently been suggested that the numerical coefficient in Eq. (9) may be incorrect (Ref. 21). The actual value of this coefficient is actually irrelevant for this work. Indeed, the microscopic exchange constants J_1-J_3 were deduced from the measured spin-wave bandwidths in $BaCu_2Si_2O_7$ using the *same* value of the coefficient. Note that it is Δ, and not the actual J values, that determines the spin-wave dispersion perpendicular to the chains in Eq. (7). Unlike the exchange parameters, which characterize the *model Hamiltonian*, Δ is a true observable physical quantity, equal to the measurable spin-wave energy at $\boldsymbol{Q}=(0.5,0.5,1)$, where interchain interactions in $BaCu_2Si_2O_7$ cancel out at the RPA level, and is thus independent of any theoretically derived constants.

[21] F.H.L. Essler (private communication).

[22] G. Muller, H. Thomas, M.W. Puga, and H. Beck, J. Phys. C **14**, 3399 (1981).

[23] M.J. Cooper and R. Nathans, Acta Crystallogr. **23**, 357 (1967).

[24] S.E. Nagler (private communication).

[25] J.-i. Igarashi and A. Watabe, Phys. Rev. B **43**, 13 456 (1991); corrected in J.-i. Igarashi, *ibid.* **46**, 10 763 (1992).